WILEY

Cladistics

Cladistics 40 (2024) 636–652

doi: 10.1111/cla.12596

Plant species diversification in the Himalaya–Hengduan Mountains region: an example from an endemic lineage of *Pedicularis* (Orobanchaceae) in the role of floral specializations and rapid range expansions

Rong Liu[a,b,c], Wei-Jia Wang[a,d], Hong Wang[c,d], Richard H. Ree[e], De-Zhu Li*[b] and Wen-Bin Yu*[a,f]

[a]*Center for Integrative Conservation and Yunnan Key Laboratory for the Conservation of Tropical Rainforests and Asian Elephants, Xishuangbanna Tropical Botanical Garden, Chinese Academy of Sciences, Mengla, Yunnan 666303, China;* [b]*Germplasm Bank of Wild Species, Kunming Institute of Botany, Chinese Academy of Sciences, Kunming, Yunnan 650201, China;* [c]*University of Chinese Academy of Sciences, Huairou District, Beijing 101408, China;* [d]*Key Laboratory for Plant Diversity and Biogeography of East Asia, Kunming Institute of Botany, Chinese Academy of Sciences, Kunming, Yunnan 650201, China;* [e]*Negaunee Integrative Research Center, Field Museum, Chicago, Illinois 60605, USA;* [f]*Southeast Asia Biodiversity Research Institute, Chinese Academy of Sciences, Mengla, Yunnan 666303, China*

Received 7 March 2024; Revised 15 August 2024; Accepted 18 August 2024

Abstract

The *c*. 270 endemic species of *Pedicularis* in the Himalaya–Hengduan Mountains (HHM) region exhibit high diversity in geographic distribution, elevational range and floral morphology. Many of these, including the species with the longest corolla tubes and beaked galeas, are monophyletic and represent a putative *in situ* radiation. In this study, we focus on the representative Clade 3 within the HHM region. We integrate the plastid phylogeny of this clade with environmental data and species distributions to infer environmental correlates of species diversity. We estimate macroevolutionary rates and reconstructed ancestral states for geographic ranges and corolla traits, and analyse patterns of range overlap and niche evolution to assess drivers of diversification in the HHM region. Our results show that the region from northwest Yunnan to southwest Sichuan is the centre of diversity for this clade of *Pedicularis*. Rates of diversification are associated with precipitation and multiple environmental factors. Multiple range expansions from the Sanjiang (Three Parallel Rivers) region, followed by allopatric speciation across the HHM region, contributed to early rapid diversification. Corolla traits are not significantly associated with species diversification. This study highlights the importance of integrated evidence for understanding species diversification dynamics and contributes to our understanding of the origins of the remarkable richness of plant species in the HHM region.

Introduction

Lineage diversification has been extensively documented in montane regions, where high biodiversity is associated with complex geographical and climatic conditions (Antonelli et al., 2018; Rahbek et al., 2019a, 2019b; Perrigo et al., 2020) that are thought to facilitate geographical and ecological speciation (Hoorn et al., 2013; Lee et al., 2015; Mulch, 2016; De Kort et al., 2020; Pepin et al., 2022). Orogeny has been associated with increased rates of diversification in several montane plants such as *Lupinus* (Leguminosae) (Drummond et al., 2012) and temperate bamboos (Ye et al., 2019). In other cases, faster diversification has been associated with traits representing adaptations, such as specialized bracts in *Saussurea* (Asteraceae) (Zhang et al., 2021), fruit type in Andean Bromeliaceae (Givnish et al., 2014) and pollination mode in bellflowers (Campanulaceae)

---

*Corresponding author:
E-mail address: dzl@mail.kib.ac.cn (D-ZL); E-mail address: yuwenbin@xtbg.ac.cn (W-BY)

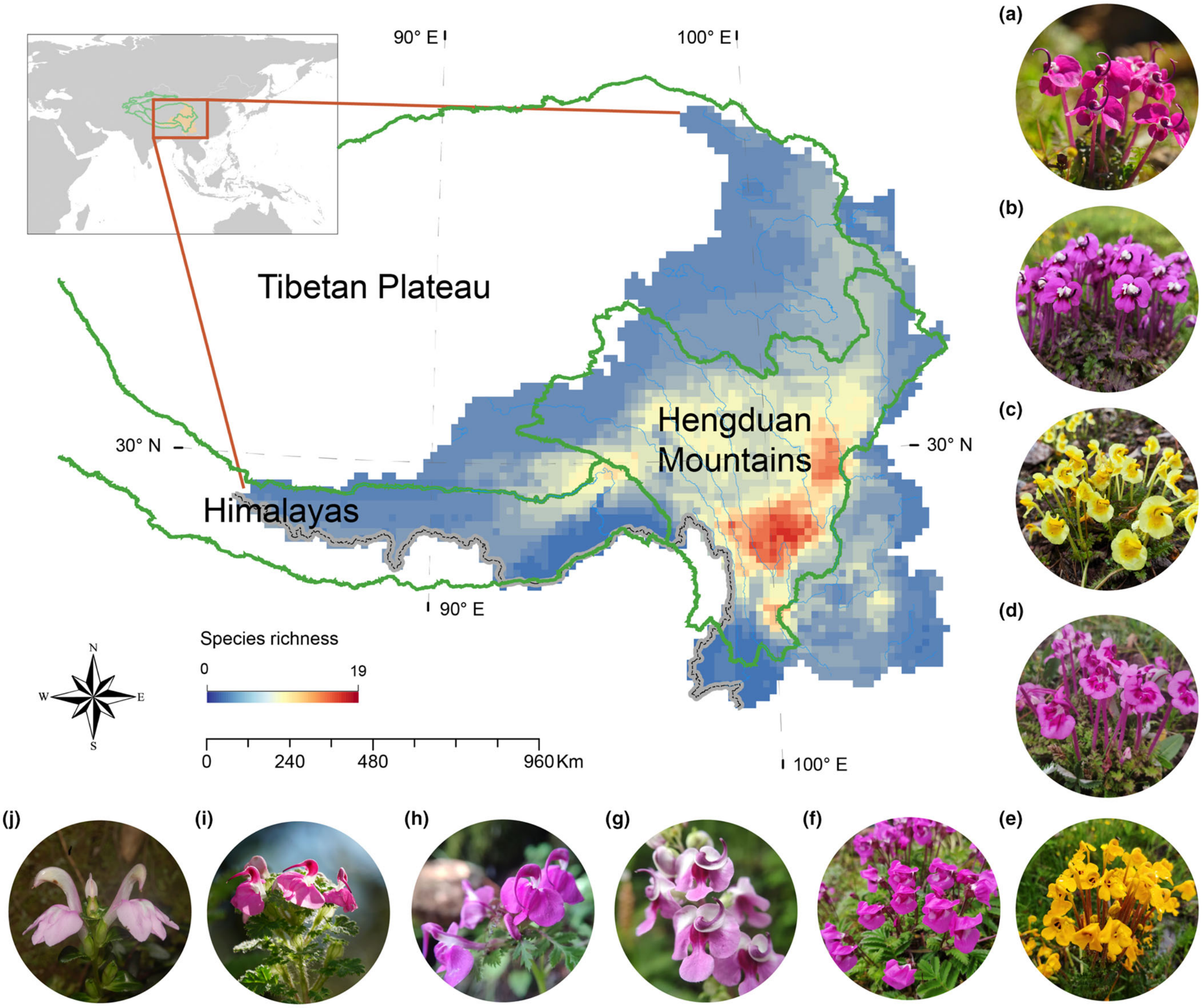

Fig. 1. Species richness pattern of *Pedicularis* Clade 3 on the Hengduan Mountains and Eastern Himalayan region with the grid cells of 20 × 20 km. The green line shows the boundary of the Hengduan Mountains region and partial Himalayas and Tibetan Plateau. The boundary refers to Liu et al. (2022a). (a) *P. sigmoidea* Franchet ex Maximowicz; (b) *P. milliana* W. B. Yu, D. Z. Li & Hong Wang; (c) *P. cranolopha* Maximowicz; (d) *P. latituba* Bonati; (e) *P. longiflora* Rudolph; (f) *P. mussotii* Franchet; (g) *P. davidii* Franchet; (h) *P. fengii* H. L. Li; (i) *P. gruina* Franchet ex Maximowicz; (j) *P. nigra* (Bonati) Vaniot ex Bonati. Photographs by: Wen-bin Yu (j), Rong Liu (a–i).

(Lagomarsino et al., 2016). A holistic understanding of diversification dynamics requires consideration of multiple factors and their potential interactions (Givnish, 2015).

The Himalaya–Hengduan Mountains (HHM, Fig. 1) region is characterized by high species richness and endemism. Its vascular flora includes over 12 000 species, one of the richest in the Northern Hemisphere (Wu, 1988; Boufford, 2014; Yu et al., 2020). *In situ* diversification has contributed substantially to the buildup of species richness in the region since the Oligocene, probably driven by the joint effects of orogeny and onset of the Asian monsoon (Xing and Ree, 2017; Ding et al., 2020). The monsoon, which developed from the middle to late Miocene as a consequence of mountain development (Farnsworth et al., 2019), contributed to topographic relief through erosion-driven incision of major river valleys, potentially dividing the HHM region into multiple subregions with varying degrees of connectivity (Clark et al., 2005; Nie et al., 2018; Cao et al., 2022) and increasing the isolation of high-elevation “sky islands” (He and Jiang, 2014), promoting the geographical isolation and speciation of alpine lineages (Zhang et al., 2019). Prior studies have mainly focused on comparing the rates and times of lineage diversification between the Hengduan

Mountains (HDM) and adjacent regions (Xing and Ree, 2017; Ding et al., 2020; Mo et al., 2022; Xia et al., 2022; Chen et al., 2023). In contrast, there has been little exploration of the dynamics of diversification within this region.

The genus *Pedicularis* L. (Orobanchaceae) contains more than 600 species, approximately two-thirds of which are found in the HHM region (Li, 1948, 1949; Tsoong, 1955, 1956; Yu et al., 2015). Species occur in a wide range of habitats, including forests, meadows and wetlands, from valley slopes at low elevations, to alpine subnival belts above the tree line. *Pedicularis* is known for dramatic interspecific variations in corolla structure and shape, especially the galea (hood-like upper lip) being elongated into a beak that varies in length and curvature, and the corolla tube varying from short to longer than 11 cm (e.g. *P. decorissima* Diels). Despite diverse floral types in *Pedicularis*, bumblebees are the primary pollinator, and the behaviour of bumblebees is considered to be associated with the floral types (Macior, 1982; Wang and Li, 1998; Robart, 2005; Huang and Shi, 2013). Typically, beakless species offer nectar as a reward for bumblebees, whereas beaked species offer only pollen. Ethological isolation mediated by floral structure has been proposed as a key mechanism for the coexistence of sympatric *Pedicularis* species (Grant, 1994a, 1994b; Yang et al., 2007; Eaton et al., 2012). Phylogenetic analyses have revealed a striking pattern of parallel evolution in corolla traits within *Pedicularis*. For instance, the beaked galea was independently gained three times and lost more than 20 times; long corolla tubes evolved at least 21 times (Ree, 2005; Yu et al., 2015).

To investigate the diversification dynamics of *Pedicularis*, this study focuses on a clade discovered in molecular phylogenetic analyses, informally labelled Clade 3 (Yang et al., 2003; Ree, 2005; Tkach et al., 2014; Yu et al., 2015). It includes approximately 85 species (see Table S1) with diverse floral types, including many long-tubed and twisted-beak species. The majority are native to the HHM region. This combination provides an opportunity to investigate diversification dynamics in the context of biogeographical history and corolla trait evolution. First, we hypothesized that the high species diversity of *Pedicularis* within the HHM region is associated with the mountain uplift and the strengthening of the Asian monsoon. Second, we hypothesized that recently diverged species should have allopatric distributions reflecting geographic speciation, because *Pedicularis* is not obviously adapted for long-distance dispersal and the rugged topography of the HHM region should promote geographic isolation (Ren et al., 2010; Li et al., 2012). Finally, we hypothesized that the evolution of corolla traits primarily promotes species coexistence as a response to the high species diversity (Armbruster and Muchhala, 2009; Armbruster, 2014), rather than directly facilitating reproductive isolation, thus contributing to the speciation process. Therefore, we do not expect changes in corolla traits to match shifts in diversification rates.

With these hypotheses, the main goals of this study are to reconstruct the phylogeny of *Pedicularis* Clade 3 and integrate corolla traits, species distribution information and environmental data to investigate: (i) speciation and extinction rates; (ii) the diversification process associated with the evolution of corolla traits; and (iii) the lineage diversification rates in the context of historical biogeography within the HMM region.

Materials and methods

Taxon samplings and sequencing

We sampled a total of 91 individuals representing 52 accepted species, four undescribed new species and four undescribed taxa that are morphologically related to accepted species of *Pedicularis* from Clade 3 (i.e. *P. amplituba* H.L. Li, *P. sigmoidea* Franch., *P. cephalantha* Franch. ex Maxim and *P. davidii* Franch.) (Table S1). Additionally, we sampled one individual of *P. axillaris* Franch. ex Maxim., the sister species to Clade 3. Total genomic DNA of new samples was extracted from leaf tissues using a CTAB method (Pahlich and Gerlitz, 1980). For some rare species, DNA extraction was performed using herbarium specimens. The purified DNA was then fragmented to approximately 200–500 bp in size by sonication, and libraries were constructed using the NEBNext Ultra II DNA Library Prep Kit for Illumina (Illumina, San Diego, CA, USA). Each sample was sequenced using the Illumina Hi-Seq 2500 platform, generating pair-end reads of 150 bp length, with a minimum of 2.5 Gb raw data per sample.

Based on current phylogenetic frameworks of Orobanchaceae (McNeal et al., 2013; Yu et al., 2018a; Jiang et al., 2022) and *Pedicularis* (Ree, 2005; Tkach et al., 2014; Yu et al., 2015), we chose four representative genera of Orobanchaceae (*Lindenbergia philippensis* (Chum.) Benth., *Rehmannia elata* N. E. Brown, *Triaenophora shennongjiaensis* X. D. Li, Y. Y. Zan & J.Q. Li and *Phtheirospermum japonicum* (Thunb.) Kanitz), *Pedicularis tongolensis* Franch. from Clade 5 and *P. axillaris* sister to Clade 3 and *Wightia speciosissima* (D. Don) Merr. of Wightiaceae as the outgroup (Table S2). The plastomes of four genera of Orobanchaceae (National Center for Biotechnology Information, NCBI accession numbers HG530133, KX636161, MH071405 and MN075943) plus *P. tongolensis* (MZ264887) and *W. speciosissima* (MK381318) were downloaded from the NCBI GenBank (Table S2).

Plastid genome assembly and annotation

Complete and circular plastid genome sequences were assembled *de novo* using the GetOrganelle toolkit (Jin et al., 2020) and assembly graphs were visually checked using Bandage (Wick et al., 2015). Samples with incomplete assemblies were scaffolded in Geneious version 11.0 (Kearse et al., 2012) using the plastid genome of *P. tongolensis* as the reference. All plastid genomes were then annotated using the PGA script (Qu et al., 2019), followed by manual adjustments in Geneious using the plastid genome of *P. japonicum* as the reference, for which no pseudogenes are known (Li et al., 2021b). Detailed information on all the plastid genome sequences can be found in Table S2.

Phylogenetic analyses

Phylogenetic analyses were inferred using the concatenated coding sequence (CDS) dataset and the whole plastid genome dataset. Whole plastome sequences with one inverted repeat (region were aligned using MAFFT 7.0 (Katoh et al., 2019). For the CDS dataset, we retained a total of 67 functional coding sequences (CDS). Each CDS was aligned using MAFFT 7.0, then they were concatenated into a supermatrix in Geneious. We removed alignment gaps for both datasets using trimAl with the parameter as “-gt 0.9 -cons 60” (Capella-Gutierrez et al., 2009). Maximum likelihood (ML), maximum parsimony (MP) and bayesian inference (BI) methods were used to reconstruct the phylogeny. We inferred the ML tree using RAxML 8.2.10 with the GTR + Γ model for the plastome dataset and by the partition parameters of each CDS for the CDS dataset, respectively (Stamatakis, 2014). Node support values (maximum likelihood bootstrap, MLBS) were estimated from 1000 bootstrap replicates. An MP tree was inferred using TNT 1.6 (Goloboff et al., 2008; Goloboff and Morales, 2023). The search strategy consisted of heuristic searches using 2000 replications of random addition, followed by tree bisection reconnection branch-swapping, retaining two trees per replication. A strict consensus tree was generated from the most parsimonious trees. Node support values (maximum parsimony bootstrap, MPBS) were estimated by bootstrap resampling with 1000 replicates. The BI analysis was conducted using MrBayes 3.2 (Ronquist et al., 2012). The best-fit substitution model was estimated using jmodeltest2 (Darriba et al., 2012). Markov chain Monte Carlo (MCMC) was set at 5 million generations with two simultaneous runs, each comprising four incrementally heated chains. The BI analysis was started with random trees and sampled every 100 generations. The values of the average standard deviation of split frequencies (<0.005) and potential scale reduction factor of convergence diagnostics (= 1.00) were used to determine the convergence. The first 25% of trees were discarded as burn-in, and a majority-rule consensus tree was generated from the remaining trees.

Divergence time estimation

The concatenated CDS matrix was imported into BEAST 1.10.4 (Suchard et al., 2018) for the estimation of divergence times. Since no reliable fossil records are known within Orobanchaceae, two secondary calibration points established by Yu et al. (2018a) were used to estimate the divergence time of *Pedicularis* Clade 3. First, all samples of Orobanchaceae were defined as the monophyletic group and *W. speciosissim* was the outgroup; then all *Pedicularis* samples and *P. japonicum* were designated as the monophyletic group. The crown ages of these two monophyletic groups were specified as 54.56 (44.37–65.30) Ma and 35.38 (24.69–46.41) Ma with a normal distribution, respectively. The MCMC sampling was conducted with 100 million generations, sampled every 1000 generations. The substitution model was set as GTR + Γ, the clock model was set as a log–normal relaxed clock and the speciation process was set as the Yule model. The MCMC analysis was conducted three times, independently. The output of BEAST was evaluated using Tracer (Rambaut et al., 2018) to confirm convergence using the criterion of effective sample size >200. After discarding 25% of the initial trees as burn-in, the maximum clade credibility tree with median node height was generated using TreeAnnotator 1.10.4 (Suchard et al., 2018).

Species distribution, corolla traits and environmental variables

Species distribution data for the sampled taxa were obtained from multiple sources, including the Chinese Virtual Herbarium (https://www.cvh.ac.cn/), the Global Biodiversity Information Facility (https://www.gbif.org/), the Biodiversity of Hengduan Mountains website (https://www.hengduan-biodiversity.net/fieldnotes), the Plant Photo Bank of China (https://ppbc.botanicalgarden.cn:8888/) and the Chinese Field Herbarium (https://www.cfh.ac.cn/). Each specimen or photo record was carefully checked against the type specimen in the JSTOR Global Plants database (http://plants.jstor.org/) to verify accuracy of identifications. The voucher locations were recorded at least to the level of town or village; records without exact location were discarded. The distribution information of unknown and undescribed taxa that were sampled was mainly obtained from collection record and our field survey. Detailed information and locality records are presented in Table S3.

Morphological characters of the corolla beak and tube length for sampled species were primarily obtained from Flora of China (electronic version, http://www.efloras.org/). The midpoints of reported values in corolla traits were collected for analyses (refer to Table S4 for detailed information). The corolla tube length was then coded as a categorical variable with two states, short and long, with a cutoff of 25 mm (Table S4) following the approach used by Ree (2005). Meanwhile, based on the division approach used by Ree (2005), we also scored four categorical states for the corolla galea: (i) no beak; (ii) short (less than 4 mm) and straight beak; (iii) long (greater than 4 mm) and curved beak; and (iv) long and S-shaped or twisted beak.

We collected environmental data using 24 environmental variables that capture aspects of bioclimate, topography, vegetation and hydrology. These include: 19 bioclimate factors from the WorldClim dataset (Fick and Hijmans, 2017), with a spatial resolution of 2.5 arc-min; two topographical factors (slope and elevation) extracted from a digital elevation model with a spatial resolution of 30 m (http://www.gscloud.cn/home); the normalized difference vegetation index (NDVI), a measure of vegetation greenness and density, at a spatial resolution of 3 arc-min (http://data.tpdc.ac.cn/en/); and the potential evapotranspiration and aridity index, representing the amount of water that could potentially be evaporated and transpired by plants under prevailing climate conditions, and the dryness of the environment. The potential evapotranspiration and aridity index were acquired from a source with a spatial resolution of 30 arc-sec (https://cgiarcsi.community).

Spatial patterns and environmental correlates of species richness

To quantify the modern spatial patterns of species richness in *Pedicularis* in the HHM region, we first partitioned the digital elevation model raster of the study area into 20 × 20 km grid cells using ArcGIS 10.2. Species occurrence records were assigned to the corresponding grid cells. We determined the geographic distribution of each species by applying the least concave polygon method implemented in ArcGIS 10.2. Then, the grid cells within each distribution polygon were filtered based on the elevation information described by each species in eFloras. Patterns of species richness were obtained from the superposition of species distributions.

Mean values of all 24 environmental variables were computed for each grid cell. We tested for collinearity using the variance inflation factor and variables with variance inflation factor values <5 were retained. Seven environmental factors (slope, elevation, aridity index, NDVI, Bio4 (temperature seasonality), Bio14 (precipitation of driest month) and Bio15 (precipitation seasonality)) were retained for further analyses. To explore the relationship between these environmental factors and species richness, we constructed a generalized linear model and a spatial autoregressive model in which species richness was the response variable and the environmental factors were predictors. To assess the adequacy of the regression models and examine potential spatial autocorrelation in the residuals, Moran’s *I* test was performed on the residuals of the regression analysis. Moran’s *I* was calculated using the R package “spdep” (Bivand and Wong, 2018) with the function “lm.morantest”. This test helps determine whether the residuals exhibit any spatial clustering or autocorrelation. The relationships between the predictors and the dependent variable (species richness) were visualized using partial-residual plots generated using the R package “car” (John and Sanford, 2019) with the function “crPlots”.

Geographical patterns of sister species

To quantify the geographical patterns of recent divergences in *Pedicularis*, we assessed the extent of geographical range overlap between sister species pairs, based on grid cell occupancy. Initially, we computed the values of absolute range overlap divided by the range size of each species. These values were averaged to obtain the average percentage of overlap for each sister species pair. However, this might overestimate the degree of distribution range overlap owing to the masking of potential differences in microhabitat or elevational range. Therefore, to estimate the elevational difference between the sister species pair, we calculated the phylogenetic signal of elevation using the midpoint value of elevation range data from the Flora of China (Table S4). Blomberg’s K and Pagel’s λ were computed using the R package phytools (Revell, 2012), with the function “phylosig”, and “traitgram” (Revell, 2013) was used to estimate the ancestral states of elevation using the R package “phytools” with the function “phenogram”.

Macroevolutionary rate estimation

To estimate rates of diversification, we used BAMM (Bayesian Analysis of Macroevolutionary Mixtures) (Rabosky et al., 2014). Duplicated tips of ingroup species and outgroups in the time tree were first removed using the R package “ape” (Paradis et al., 2004) with the “drop.tip” function. For BAMM analysis, we specified global sampling fractions of 0.65 (sampled species: 60/total species: 92) (Table S1) to account for the remaining unsampled species (Rabosky, 2014). Prior probability distributions were parameterized using the “setBAMMpriors” function in the R package “BAMMtools” (Rabosky et al., 2014). The MCMC run was set to 20 million generations. The initial 10% of samples from the MCMC run were discarded as burn-in. The R package “CODA” (Plummer et al., 2006) was used, specifically the “effectiveSize” function, to assess the coverage of the MCMC chains. An effective sample size >200 was used as a criterion for convergence. Posterior probabilities of diversification rates through time were extracted and summarized using BAMMtools.

To complement the BAMM results, multiple treewide time-dependent diversification models were tested using the R package “RPANDA” (Morlon et al., 2016) with the function “fit_bd”. Four kinds of models were fit: (i) a pure birth model with a constant speciation rate; (ii) a pure birth model with a variable (linear and exponential) speciation rate; (iii) a model with variable (linear and exponential) speciation rate and a constant extinction rate; and (iv) a model with a variable (linear and exponential) speciation rate and a linear extinction rate. The model with the lowest corrected Akaike information criterion (AICc) was considered the best fit. To estimate the effect of historical environmental changes on speciation and extinction rates, a time-dependent model with a palaeoenvironment variable was built using the RPANDA function “fit_env”. The focus of this analysis was on the historical changes of annual precipitation (mm) of East Asia, which was derived from a general circulation model with geological data (Farnsworth et al., 2019).

To test whether features of the corolla covary with diversification rates, we used the MuSSE (Multi-State Speciation and Extinction) model implemented in the R package “diversitree” (FitzJohn, 2012). Seven states were coded, representing different combinations of beak type and tube type (i.e. I, beakless with a short tube; ii, short beak with a short tube; iii, curved beak with a short tube; iv, S-shape beak with a short tube; v, short beak with a long tube; vi, curved beak with a long tube; and vii, S-shape beak with a long tube). In MUSSE analyses, dual transition of corolla trait was disallowed (detailed in Table S5). Based on AIC value, we compared the fit of multiple models where speciation and extinction rate change vary with different corolla type with those where the trait is independent of the speciation and extinction process. For the null model, priors were set to equal rates of speciation (λ), extinction (μ) and transition (q) across all states. Five alternative models were tested: (i) λ, μ and q rates are all different; (ii) λ rates are different, μ and q are equal; (iii) μ rates are different, λ and q are equal; (iv) λ and μ rates are different, q is equal; and (v) q rate is different, λ and μ are equal. The MuSSE model was run with a MCMC sampling of 5000 steps, with the first 1000 steps discarded as burn-in.

Ancestral range reconstruction

To estimate the biogeographical history of *Pedicularis* Clade 3 in the HHM region, ancestral range reconstruction was conducted using the dispersal–extinction–cladogenesis (DEC) model (Ree and Smith, 2008; Ree and Sanmartín, 2018) in the software RevBayes (Höhna et al., 2016). We adopted the six floristic subregions proposed in Wu et al. (2010): (A) Central Yunnan Plateau; (B) Southern HDM; (C) Sanjiang Valley; (D) Northern HDM; (E) Eastern Himalaya; and (F) Upper Brahmaputra River. More recently, the floristic structure of the HHM region has been studied using quantitative data-driven methods (Zhang et al., 2016; Liu et al., 2021; Li et al., 2021a), and this produced similar regionalization schemes. In the RevBayes analysis, dispersal and extirpation rates were assumed to be constant across areas. The MCMC run was set to 3000 generations. The R package “RevGadgets” (Tribble et al., 2022) was used to visualize the result.

Reconstruction of ancestral corolla traits

To estimate ancestral states of the corolla galea, we used a hidden rate model of discrete character evolution. Hidden rate models allow different evolutionary rate classes to be associated with latent or unobserved (“hidden”) states (Beaulieu et al., 2013). As mentioned above, four types of corolla galea were coded as: (i) beakless type; (ii) straight beak; (iii) curved beak; and (iv) S-shaped beak. Inference was carried out using the R package “corHMM” (Boyko and Beaulieu, 2021) with the function “corHMM”. Three rate classes (time homogeneous, two hidden rate, and three hidden rate) with equal-rate, symmetrical rate (SR) and all-rates-different transition models, were fit to the data. The model with the lowest AICc value was selected as the best model.

The corolla tube length displays wide variations, varying from 5 to 120 mm. Three evolution models for the continuous trait, Brownian motion (BM), Ornstein–Uhlenbeck and Early burst model were used to estimate the ancestral state of corolla tube length. Model fitting was estimated using the R package “geiger” (Pennell et al.,

Fig. 2. Maximum likelihood (ML) tree of *Pedicularis* Clade 3 inferred from concatenated 67 plastid concatenated coding sequence (CDS) matrix. The left tree shows the topology of the ML tree. Numbers associated with the branches are ML, maximum parsimony (MP) bootstrap value (MLBS and MPBS), and bayesian inference posterior probabilities (BIPP), and unmarked branches mean MLBS/MPBS/BIPP >95/95/0.95. Photographs by: Wen-Bin Yu (F, M, N, S and X), Rong Liu (A–E, G–K, O–R, T, U and W), Wei-Jia Wang (V) and Qin Tian (L).

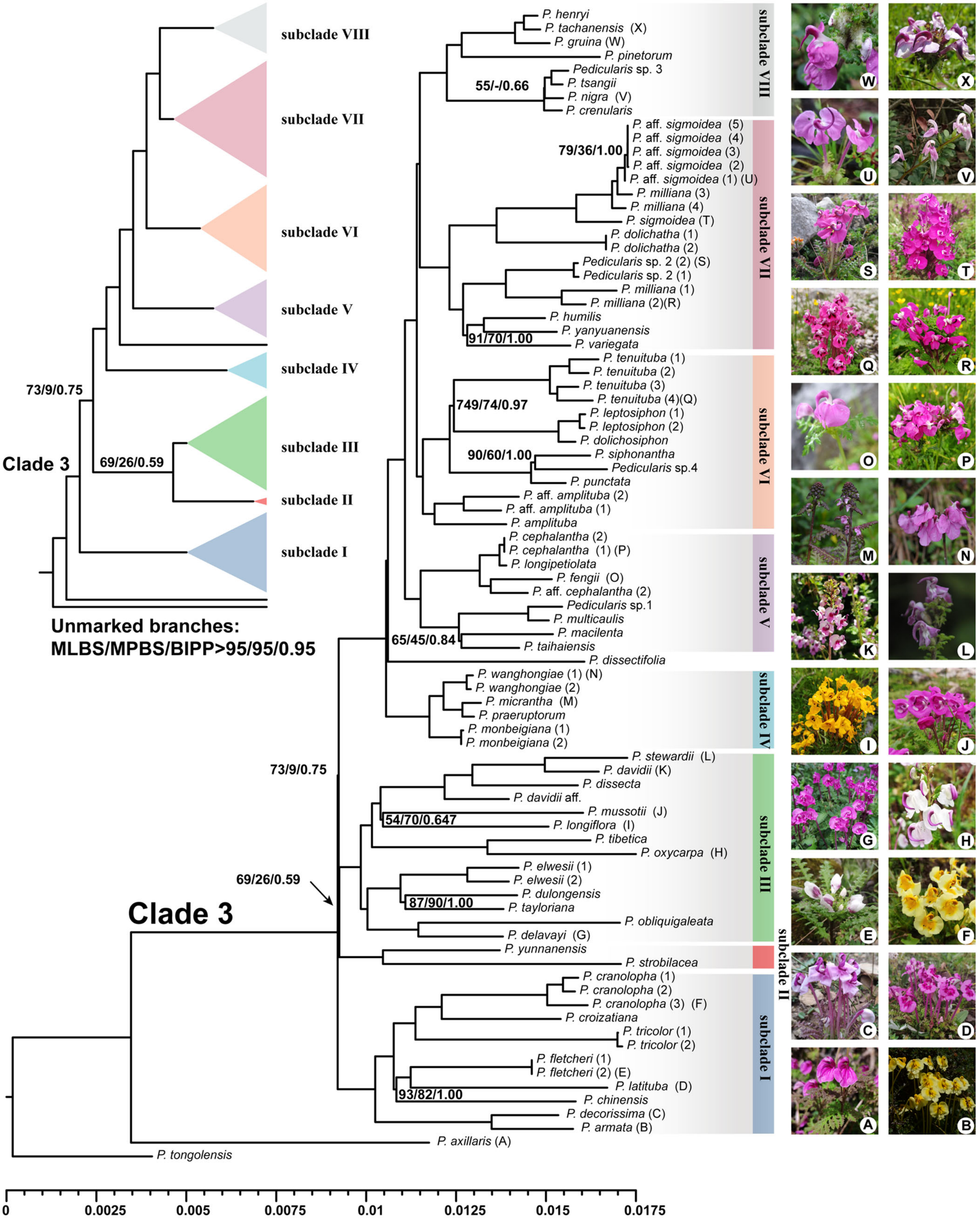
subclade VIII
subclade VII
subclade VI
subclade V
subclade IV
73/9/0.75
subclade III
Clade 3
69/26/0.59
subclade II
subclade I
Unmarked branches:
MLBS/MPBS/BIPP>95/95/0.95
P. henryi
P. tachanensis (X)
P. gruina (W)
P. pinetorum
Pedicularis sp. 3
55/-/0.66
P. tsangii
P. nigra (V)
P. crenularis
P. aff. sigmoidea (5)
P. aff. sigmoidea (4)
79/36/1.00
P. aff. sigmoidea (3)
P. aff. sigmoidea (2)
P. aff. sigmoidea (1) (U)
P. milliana (3)
P. milliana (4)
P. sigmoidea (T)
P. dolichatha (1)
P. dolichatha (2)
Pedicularis sp. 2 (2) (S)
Pedicularis sp. 2 (1)
P. milliana (1)
P. milliana (2)(R)
P. humilis
P. yanyuanensis
91/70/1.00
P. variegata
P. tenuituba (1)
P. tenuituba (2)
P. tenuituba (3)
749/74/0.97
P. tenuituba (4)(Q)
P. leptosiphon (1)
P. leptosiphon (2)
P. dolichosiphon
90/60/1.00
P. siphonantha
Pedicularis sp.4
P. punctata
P. aff. amplituba (2)
P. aff. amplituba (1)
P. amplituba
P. cephalantha (2)
P. cephalantha (1) (P)
P. longipetiolata
P. fengii (O)
P. aff. cephalantha (2)
Pedicularis sp.1
P. multicaulis
P. macilenta
65/45/0.84
P. taihaiensis
P. dissectifolia
P. wanghongiae (1) (N)
P. wanghongiae (2)
P. micrantha (M)
P. praeruptorum
P. monbeigiana (1)
P. monbeigiana (2)
73/9/0.75
P. stewardii (L)
P. davidii (K)
P. dissecta
P. davidii aff.
P. mussotii (J)
54/70/0.647
P. longiflora (I)
P. tibetica
P. oxycarpa (H)
P. elwesii (1)
69/26/0.59
P. elwesii (2)
P. dulongensis
87/90/1.00
P. tayloriana
Clade 3
P. obliquigaleata
P. delavayi (G)
P. yunnanensis
P. strobilacea
P. cranolopha (1)
P. cranolopha (2)
P. cranolopha (3) (F)
P. croizatiana
P. tricolor (1)
P. tricolor (2)
P. fletcheri (1)
P. fletcheri (2) (E)
P. latituba (D)
93/82/1.00
P. chinensis
P. decorissima (C)
P. armata (B)
P. axillaris (A)
P. tongolensis
subclade VIII
subclade VII
subclade VI
subclade V
subclade IV
subclade III
subclade II
subclade I
W
X
U
V
S
T
Q
R
O
P
M
N
K
L
I
J
G
H
E
F
C
D
A
B
0
0.0025
0.005
0.0075
0.01
0.0125
0.015
0.0175

2014) with the function “fitContinuous”. Continuous tube length was reconstructed using the R package “phytools” (Revell, 2012, 2024) with the function “contMap”, and the results of ancestral state were reflected on the branches.

Results

Plastid phylogenomics and divergent time estimations

Of the 92 samples, 80 yielded complete plastid genomes using GetOrganelle, three samples were manually assembled using a reference genome and nine samples were discarded owing to low assembly quality. Plastome size varied from 142 059 to 152 136 bp. With six samples from the NCBI, 89 samples representing 68 taxa (including 60 species from Clade 3) were included in the final dataset. Examination of the plastome data revealed strong pseudogenization and loss of the NA(D)H dehydrogenase-like (NDH) genes, as well as pseudogenes in *accD*, and *ccsA*. Detailed information on this can be found in Table S2. The concatenated alignment of 67 coding sequence (CDS) regions comprised 55 214 bp in length including 10 234 variable sites and 5817 parsimony informative sites. In addition, the plastome data comprised 115 392 bp in length including 28 023 variable sites and 15 908 parsimony informative sites.

Both the plastome (Fig. S1) and CDS datasets (Fig. 2, Figs S2–S4) yield consistent topologies including eight well-supported clades (labelled here as subclade I to subclade VII), with an expectation that the subclade II was weakly supported as sister to subclade I + subclades IV–VIII (MLBS = 56) in the plastome dataset or sister to subclade III (MLBS = 69) in the CDS dataset. Based on the CDS dataset, the ML, MP and BI analyses produced consistent topologies with maximum support values for most of the nodes (Fig. 2, Figs S2–S4). In all topologies, eight major clades are fully supported (MLBS/MPBS/BIPP = 100/100/1.00). Support values for deeper divergences are weak in some cases, e.g. the most recent common ancestor (MRCA) node of subclade II + subclade III (MLBS/MPBS/BIPP = 69/26/0.59). The MRCA of subclade II + subclade III and the remaining clades showed moderate support (MLBS/MPBS/BIPP = 73/9/0.75). In addition, four undescribed species showed a unique phylogenetic position to their affinis, such as *P.* aff. *cehalantha* is sister to *P. fengii*, and *P.* aff. *davidii* is sister to *P. dissecta* + *P. davidii* + *P. stewardii*.

The crown age of Clade 3 was estimated to be 20.24 Ma, with a 95% highest posterior density (HPD) interval of 16.15–25.75 Ma (Fig. S5). The crown ages of major clades within Clade 3 were estimated as follows: Subclade I at 12.04 Ma (95% HPD, 9.58–14.75 Ma), subclade II at 10.57 Ma (HPD, 6.94–14.16Ma), subclade III at 12.62 Ma (95% HPD, 10.28–15.27 Ma) and the MRCA of subclades IV–VII at 11.64 Ma (95% HPD, 9.46–14.04 Ma).

Species diversity patterns in the HHM region

The distribution of species richness within Clade 3 exhibited a strong geographical signal, with the Southern HDM having the highest richness (Fig. 1). This pattern is consistent with regionalization schemes proposed by Wu et al. (2010), in which Region B (i.e. subregion E14b in Wu et al., 2010, hereafter), referred to as the Southern HDM, is considered the biodiversity richness centre of the HDM flora.

Species richness exhibits strong spatial autocorrelation (Moran’s $I = 0.86$), so we used a spatial autoregressive model. Among the seven environmental factors examined, three climate-related factors (Bio4, Bio14 and Bio15) were negatively related to species richness, while two topographical factors (elevation and slope) and two other factors (aridity index and NDVI) were positively related (Fig. 3a–h and Table 1). This suggests that species richness is correlated with the combination of climate, topography and other environmental factors in the HHM region.

Phylogenetic patterns of geographic range overlapping

The geographic ranges of sister species were predominantly allopatric (Fig. 4 and Table S6) with some exceptions. For example, *P. tenuituba*, *P. leptosiphon* and *P. dolichosiphon* show overlapping distributions, which may have arisen following secondary contact (Liu et al., 2022b). Estimates of phylogenetic signal in elevational midpoint values (Fig. S6) (Blomberg’s $K = 0.55$, $P = 0.061$, and Pagel’s $\lambda = 0.74$, $P < 0.0001$) indicated relatively higher divergence of elevation distribution among species than expected from their evolutionary relationships. For examples, in the sister pair of *P.* aff. *cephalantha* and *P.* aff. *fengii* (overlap index = 0.317), the former is mainly found at elevations between 4000 and 4500 m, but the latter mainly occurs at elevations between 3800 and 4200 m.

Variations of macroevolutionary rates

Net diversification rate, as estimated by BAMM, increased over the period 20–15 Ma and decreased thereafter (Fig. 5). A similar pattern was inferred using RPANDA (Table S7). Under the palaeoenvironment-dependent diversification model in RPANDA, a positive correlation was found between the net diversification rate and historical onset of the Asian monsoon (Fig. S7).

The MuSSE analysis showed the lowest AICc for the null model (equal rate of λ, μ and q) (Table 3), indicating that corolla type is not significantly associated with variation in the diversification rate.

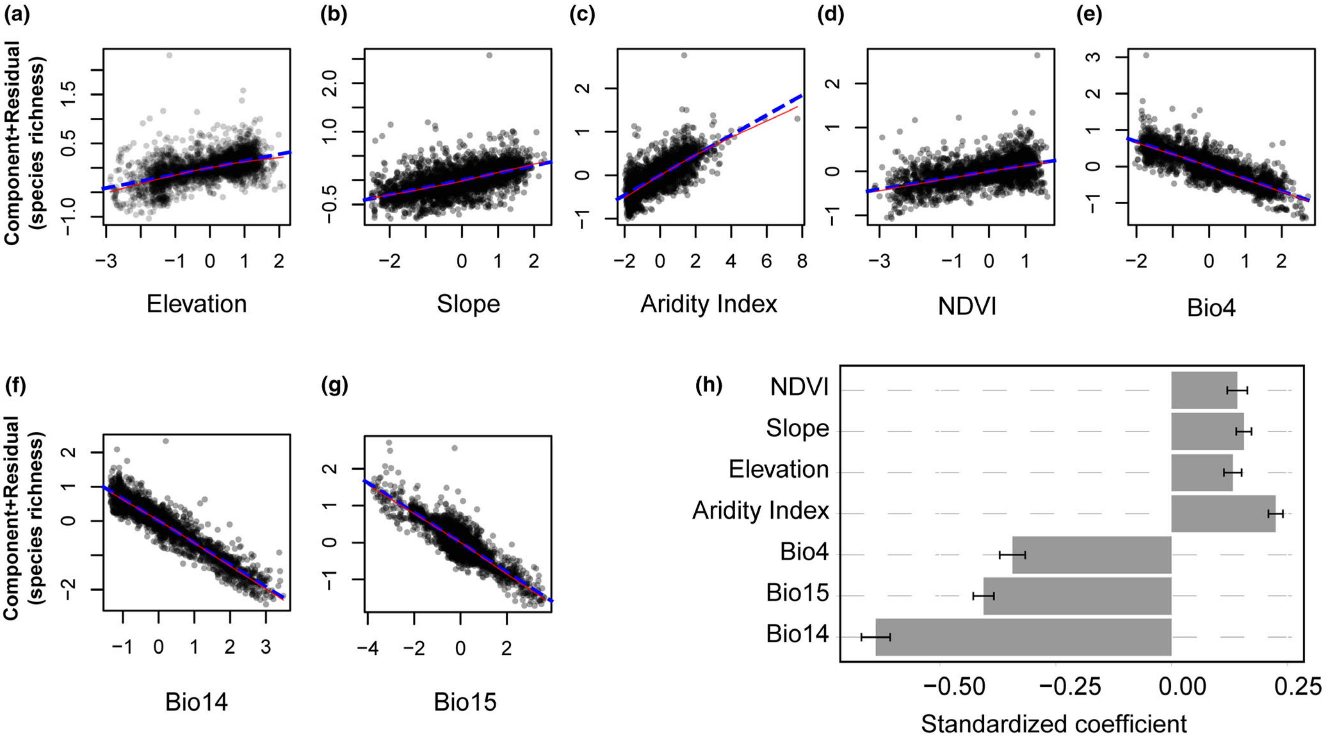

Fig. 3. Relationships between environmental predictor variables and species richness based on the spatial autoregressive model (a–g). DNVI, Normalized Difference Vegetation Index; Bio4, Temperature seasonality; Bio14, Precipitation of driest month; Bio15, Precipitation seasonality. (h) The relative importance of seven environmental factors. The red line shows the actual residuals, and blue dotted line shows the expected residuals; the overlap of the blue line and the red line shows the linear relationship between the predictors and the dependent variable.

Table 1
Summary of generalized linear model and spatial autoregressive model explaining species richness of *Pedicularis* Clade3 within 20 × 20 km grid cells

	Generalized linear model		Spatial autoregressive model	
	Estimate	Error	Estimate	Error
Intercept	1.42***	0.01	1.32***	0.01
Mean elevation	0.23***	0.01	0.132***	0.02
Mean slope	0.16***	0.01	0.16***	0.02
Aridity index	0.10***	0.01	0.22***	0.02
Normalized difference vegetation index	0.24***	0.01	0.14***	0.02
Bio4	−0.33***	0.01	−0.34***	0.03
Bio14	−0.30***	0.01	−0.64***	0.03
Bio15	0.20***	0.01	−0.41***	0.02
Moran's I	0.86		0.13	
Akaike information criterion	14 992		12 227	

Significance levels: ***$P < 0.001$.

Reconstruction of ancestral regions in the HHM region

Estimates of ancestral geographic range using RevBayes (Fig. 6a) exhibited considerable uncertainty. At the root node, the most probable geographic range and probability are: BCD, 0.155; C, 0.15; and CD, 0.11. Deep nodes were primarily distributed in Region C (E14a, Sanjiang Valley subregion) with subsequent dispersal events to other regions. For example, dispersal from Region C to Region B (E14b, Southern HDM subregion) occurred at least three times. The reversal from Region B to Region C was hardly observed. Subclades VII and VII originated in Region B and subsequently colonized Region A (E13a, middle Yunnan Plateau subregion). In contrast, immigration events between Region B and Region A were frequent, and vicariance events contributed to the divergence of related species (e.g. *P. humilis* and *yanyuansis*; *P. milliana* and *Pedicularis* sp. 2).

Evolution of corolla traits

The best fit model for the evolution of corolla galea was the SR model with a time homogeneous rate (LogL = −52.67, AICc = 118.96; Table 2). Ancestral state reconstructions indicate that early ancestors of Clade 3 had a corolla with a curved beak (Fig. 6b, Fig. S8). Except for the ancestral corolla of subclade VII, which was estimated to have a S-shape beak, the ancestral corolla of the rest subclades was estimated to have a curved beak. Morphological diversification primarily occurred among the different subclades. For

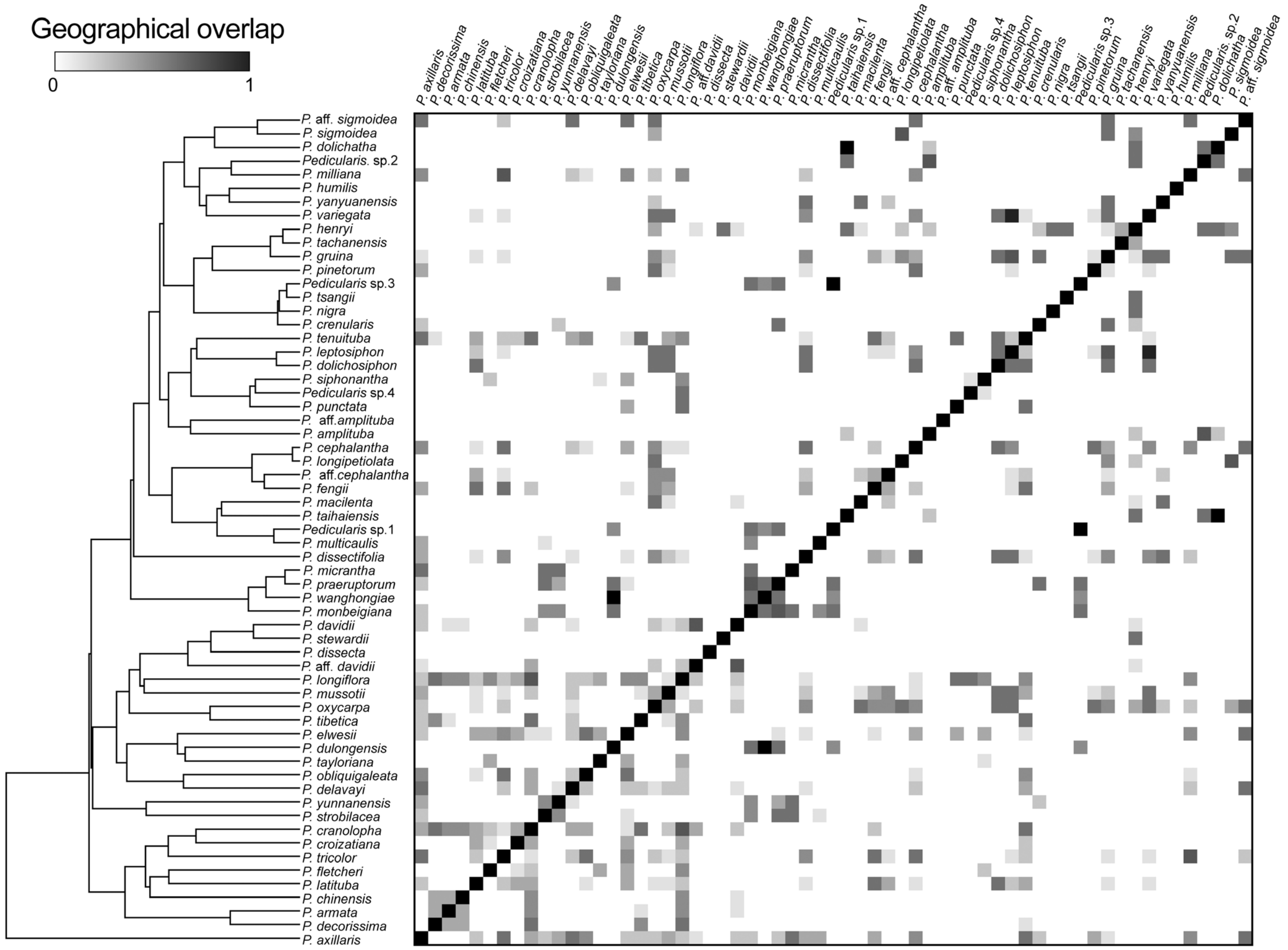

Fig. 4. Phylogenetic pattern of species overlaps. The colour gradient shifting from light to dark represents the extent of overlap (0–1) between species pairs.

instance, transition from the curved beak to the S-shape beak occurred at least five times, and to the straight beak at least four times.

The best fit model for the evolution of corolla tube was the BM model (logL = –272.31, AICc = 548.82; Table 2). The reconstruction of corolla tube length indicated that the early ancestors of Clade 3 had a corolla with a short corolla tube. The evolution of a long corolla tube was estimated to have occurred at least five times, and the long corolla tube was consistently associated with the S-shaped beak.

Discussion

Diversification dynamics of Pedicularis *Clade 3 in the HHM region*

Our analyses indicate that *Pedicularis* Clade 3 experienced early rapid diversification followed by a decline in diversification rate. This pattern is commonly observed in other diverse lineages and has been discussed in previous studies (Ricklefs, 2010; Ho et al., 2011; Ho, 2020; Louca et al., 2022). One possible explanation for this "early burst" pattern is adaptive radiation into vacant ecological niches (Glor, 2010; Wellborn and Langerhans, 2015; Garcia-Porta et al., 2022), with subsequent declines in diversification rate as niches are filled (Rabosky and Lovette, 2008; Moen and Morlon, 2014; Givnish, 2015). Another is diversification driven by the uplift of mountains, as hypothesized for the Andean clades Bromeliaceae (Aguirre-Santoro et al., 2020) and Macrocarpaea (Gentianaceae) (Vieu et al., 2022). A third hypothesis is that rapid diversification might occur following the colonization of a new region, with subsequent declines in rate occurring as geographical space is filled (Toussaint et al., 2015; Skipwith et al., 2016).

The increase of the diversification rate in *Pedicularis* Clade 3 is estimated to have occurred around the middle

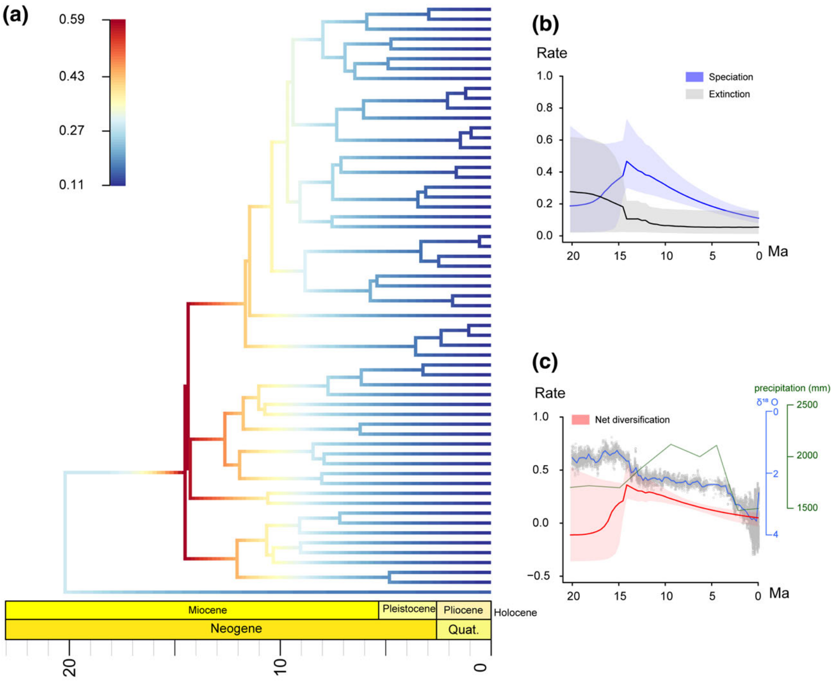

Fig. 5. Macroevolutionary rate through time among lineages of *Pedicularis* Clade 3 based on BAMM (Bayesian Analysis of Macroevolutionary Mixtures). (a) Mean phylorate plot showing model-averaged diversification rates at any point along every branch. (b) Diversification rate of speciation (blue) and extinction (grey). (c) Net diversification rate through time (red line), global palaeoclimate change (blue line) (Zachos et al., 2008) and the Asian monsoon change (green line) (Farnsworth et al., 2019).

Miocene (*c*. 15Ma). While the details of the HHM uplift history remain not fully understood, there is some consensus across various studies. Recent evidence from isotopic dating and plant fossils has shown that a large part of the HDM reached an elevation of approximately 3900 m by the early Oligocene (Su et al., 2019; Cao et al., 2022). By the early Miocene, the Himalayan region reached elevations over 5000 m (Gébelin et al., 2013; Ding et al., 2017). Historical biogeographic inferences based on molecular timetrees indicate establishment of alpine flora in the HDM by the Oligocene (Ding et al., 2020). Therefore, it is plausible that by the Miocene, the appropriate geographical and ecological conditions for the early diversification of *Pedicularis* Clade 3 were in place.

The intensification of the Asian monsoon during the middle Miocene (Farnsworth et al., 2019) is likely to have played an important role in driving the rapid diversification of *Pedicularis* Clade 3, as indicated by support for the palaeoclimate-dependent diversification model (Fig. S7). In addition to providing moisture during the summer reproductive season, intensification of the monsoon might have increased the topographic relief that is associated with allopatric speciation in mountains, as evidenced from rapid incision of major rivers during the middle to late Miocene (Clark et al., 2005; Nie et al., 2018; Spicer et al., 2020; Spicer et al., 2021; Cao et al., 2022). The predominantly allopatric distribution of closely related species (Figs 4 and 6a) suggests that speciation in *Pedicularis* has predominantly been allopatric. We hypothesize that the geographic distribution in *Pedicularis* species is generally constrained by habitat preferences and the limited range of abiotic seed dispersal. The dispersal of *Pedicularis* is unlikely across different climate zones separated by elevation. Present-day allopatry of clades older than the early Miocene could thus be explained by early range expansions before the formation of deeply incised mountains. Consequently, factors related to both orogeny and climate probably contributed to the rapid diversification of *Pedicularis* Clade 3 during the middle Miocene.

Lineage diversification plays a pivotal role in shaping the contemporary distribution of biodiversity. Instances of divergence occurring *in situ*, coupled with recurrent immigration events to Region A (E13b: Southern HDM) (see Fig. 6a), contribute to the heightened accumulation of species. Our results showed that the Southern HDM region is the biodiversity hotspot of *Pedicularis* Clade 3 (Fig. 1), where species richness is influenced by a combination of topographical, climatic and other environmental factors (Fig. 3). The wide range of habitats and climatic conditions in the Southern HDM region may be key to fostering the accumulation of species (Chang et al., 2023), thereby establishing this region as the central hub of the HDM flora (Wu, 1988; Wu et al., 2010).

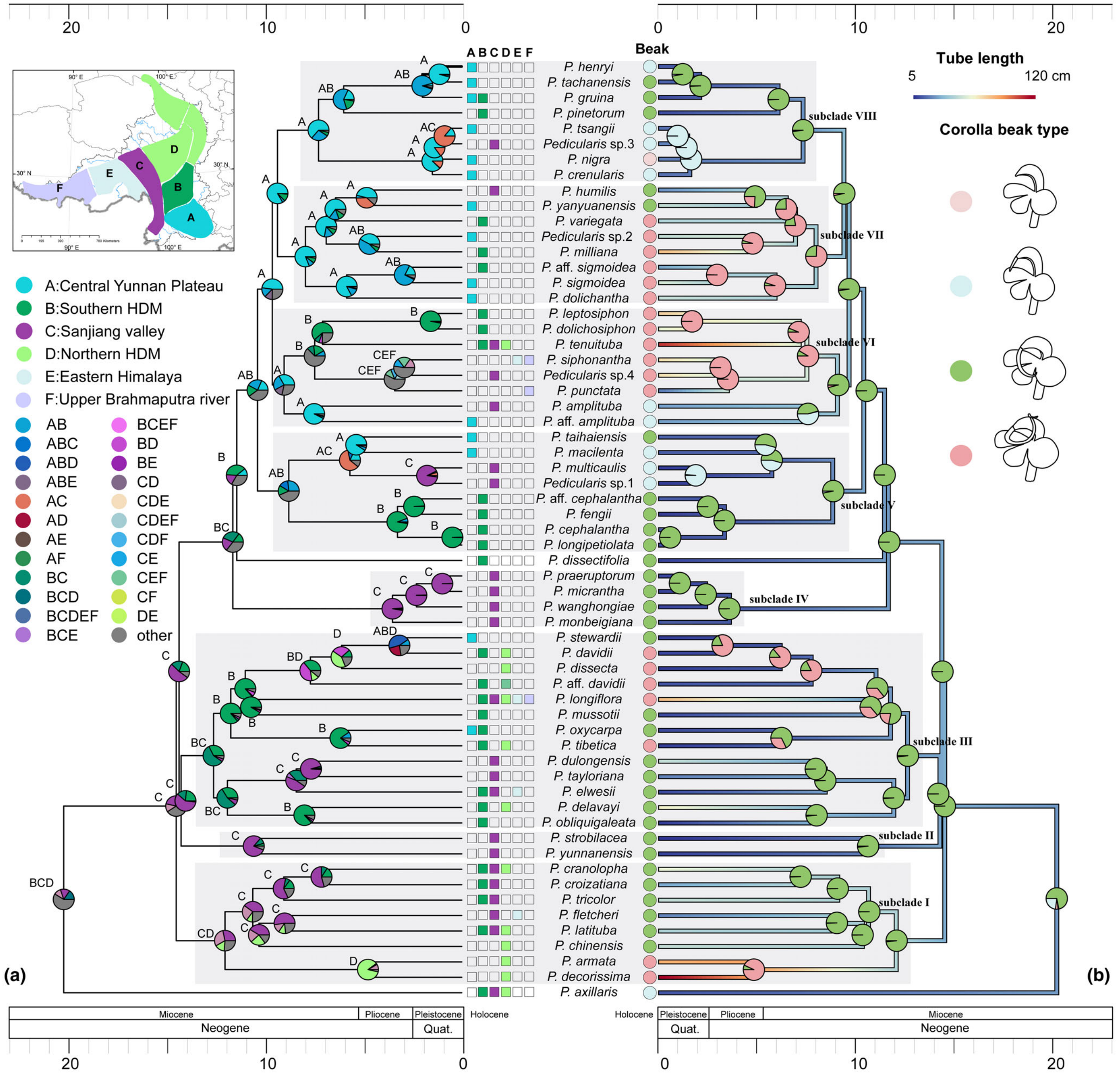

Fig. 6. Reconstruction of ancestral distribution range and corolla trait state of the *Pedicularis* Clade 3. (a) Ancestral range reconstruction based on the dispersal–extinction–cladogenesis (DEC) model. The geographical scheme of Himalaya–Hengduan Mountains (HHM) adopted from Wu et al. (2010). Pie charts at the nodes of the tree represent the relative probabilities of the ancestral range. Grey colour on the pie charts indicates other combinations of multiple areas. (b) Reconstruction of continuous corolla tube length and discrete corolla galea types. Branch colour represents the evolution of corolla tube length. Pie charts at the nodes of the tree represent the relative probabilities of the corolla galea type.

It should be noted that our phylogeny includes 60 species of Clade 3, which is 65% of 92 species in this Clade. This phylogenetic tree with its small number of species may limit our statistical power to detect shifts and correlates of diversification rate. It is worth pointing out that plastome data inferred a robust phylogenetic tree for the early rapid diversification subclade in Clade 3. For instances, subclades I, II and III, which were previously collapsed as polytomy, as well as subclades VI, VII and VIII, were resolved (Yu et al., 2015). The short corolla tube of subclade VII is now embedded into the *P. siphonantha* complex (subclades VI and VII; Yu et al., 2015; Yu et al., 2018b; Liu et al., 2022b), so that *P. siphonantha* complex is not

Table 2
Model comparison of corolla reconstruction

	Rate class	Model	LogL	AICc
Discrete trait of beak type	Time homogenous model	ER	−59.98	122.02
		ARD	−50.15	130.80
		SR	**−52.70**	**118.96**
	Rate class 2	ER	−59.21	127.13
		ARD	−47.43	188.15
		SR	−48.56	190.41
	Rate class 3	ER	−59.21	127.13
		ARD	−49.66	192.62
		SR	−51.13	139.39
Continuous trait of tube length	–	**BM**	**−272.31**	**548.82**
	–	OU	−272.31	551.03
	–	EB	−271.87	550.17

ARD, All rates different; BM, Brownian motion; EB, Early burst; ER, equal rate; logL, log-likelihood; OU, Ornstein–Uhlenbeck; SR, symmetrical rate. Bold values show the best model based on the lowest corrected Akaike information criterion (AICc) value.

supported as monophyletic herein. Thus, relying only on the plastid data cannot resolve phylogenetic confusions caused by chloroplast genome capture events. To date, topological discrepancies between nuclear and plastid datasets in *Pedicularis* have been documented in some recently derived species lineages (Yu et al., 2013; Yu et al., 2015; Liu et al., 2022b). It could be difficult to detect some potentially important diversification processes (e.g. hybridization and introgression) either plastid or nuclear data. Therefore, future studies should include more individuals from different populations and incorporate both nuclear and plastid genomic data.

Corolla trait diversification of Pedicularis *in the HMM region*

The presence or absence of nectar production in flowers and the ethological divergence of bumblebees' foraging behaviour are highly associated with corolla traits of *Pedicularis* (Macior, 1982; Ree, 2005; Robart, 2005; Wang and Li, 2005; Liu et al., 2015; Liu et al., 2016; Tong et al., 2019). The reconstruction of corolla types supports the early ancestor having had a short tube with a curved beak in *Pedicularis* Clade 3 (Fig. 6b). The curved beak galea type is associated with species exhibiting the loss of nectar production (Macior, 1982; Liu et al., 2015). The elongated beak encourages buzz-pollination behaviour in bumblebees, by requiring them to manipulate the galea to collect pollen (Macior and Ya, 1997). In the absence of nectar requiring a short corolla tube, tube length can evolve more freely in long-beaked species (Macior and Ya, 1997; Ree, 2005). The length and curvature of the corolla beak may enhance pollination accuracy and diminish interspecific reproductive interference (Harder, 1990; Huang and Shi, 2013; Armbruster et al., 2014). The importance of nectar to bumblebee behaviour has been demonstrated in experiments involving artificial supplementation (Tong et al., 2019). Repeated losses of the galea beak suggest that nectar production has re-evolved from nectarless ancestors (Ree, 2005; Yu et al., 2015). Thus, the ancestral short tube with a curved beak type holds the potential to undergo various transformations, such as elaboration of the beak to an S-shaped type, degradation into a short beak, or even complete loss of the beak. All of these transitions are inferred in our reconstruction of ancestral corolla traits.

Table 3
Comparison between null model and alternative model of MuSSE (Multi-State Speciation and Extinction) analyses

	Df	lnLik	AIC	χ^2	Pr(>|Chi|)
Null	**3**	**−312.98**	**631.95**		
All different	56	−289.29	690.58	47.37	0.69
λ free	10	−310.57	641.14	4.81	0.68
μ free	10	−310.71	641.42	4.54	0.72
λ and μ free	15	−302.65	635.31	20.64	0.06
q free	46	−290.82	673.64	44.31	0.42

Df, Degrees of freedom; lnLik, ln-likelihood. Bold values show the best model based on the lowest Akaike information criterion (AIC) value.

We did not detect differences in diversification rate associated with corolla types (Fig. 5a and Table 3). We observed that the corolla diversification appears to be associated with the geographical range expansions of early-diverging clades. Subclades that dispersed from the Sanjiang Valley region exhibit greater corolla diversity, while those that remained *in situ* retain the ancestral corolla type. The evolution of diverse corolla types in different subclades may reflect recurrent reproductive interference with other species of *Pedicularis* outside of Clade 3 (Eaton et al., 2012; Huang and Shi, 2013; Armbruster et al., 2014). Macroevolutionary analysis of the genus as a whole is needed to explore this question.

The implication of parallel range expansions

We inferred early rapid branching events and subsequent range expansions from the Sanjiang Valley region. Formed from the collision of the India-Eurasia plate, the Sanjiang orogenic belt underwent significant deformation and rotations, shifting from its original west–east to south–north orientations (Cao et al., 2019; Li et al., 2020). Historical river incision further contributed to the formation of deep valleys separating high mountains (Clark and Royden, 2000; Clark et al., 2004; Liu-Zeng et al., 2008; Nie et al., 2018). Currently, the Sanjiang Valley region is characterized by three parallel north-to-south rivers (Nu River, Lancang River and Jinsha River) and the mountain ranges (Gaoligong Mountains, Biluo Mountains and Yunling Mountains) that are divided by them. It is a corridor that enhances north–south gene flow while creating a dispersal barrier in the west–east direction (Chang et al., 2023). Biogeographical studies of multiple widespread alpine taxa have indicated historical connections between different regions related to the Sanjiang Valley region. Along both sides of the corridor, lineages or populations have shown genetic connections and divergence (Li et al., 2011; Yang et al., 2012; Luo et al., 2017; Mu et al., 2022; Rana et al., 2023). The Sanjiang Valley region may serve as a transitional area connecting the Himalayan and the HDM floristic regions.

Linear distribution ranges with low connectivity are more likely to promote population genetic divergence (TrÉNel et al., 2008; Pigot et al., 2010; Vieu et al., 2022). We hypothesize that populations of the early ancestor of *Pedicularis* Clade 3 underwent rapid divergence along the narrow Sanjiang Valley region. Before the formation of dispersal barriers, parallel geographical range expansions occurred, allowing different subclades to establish their distributions (e.g. subclade I in the Northern HDM region, and subclade V in the Central HDM region). Subsequent geographical speciation and ecological adaptation led to the modern distribution of species diversity. It may be a general pattern that plant lineages colonizing the Sanjiang Valley region before the formation of significant dispersal barriers underwent similar parallel range expansions with subsequent lineage diversification. Evidence from historical biogeographic studies across multiple taxa is necessary to test this idea.

Conclusion

The role of abiotic and biotic factors on species diversification is central to our understanding of biodiversity in mountain regions. In this study, integrative analyses showed that species diversification of *Pedicularis* Clade 3 during the middle Miocene was associated with orogeny and the intensification of Asian monsoon. Newly formed cool habitats allowed ancestors of this clade to establish a wide distribution from south to north in the Sanjing Valley region at an early stage. Floral evolution was potentially important for species coexistence following this initial radiation. Our study highlights the significance of integrating abiotic and biotic factors into evolutionary inferences to reveal the drivers of species diversification in the HHM region.

Acknowledgements

This study was supported by the National Natural Science Foundation of China (32371700, 32071670), the Strategic Priority Research Program of the Chinese Academy of Sciences (XDB31000000), Ministry of Science and Technology of China Basic Resource Investigation Program (2021FY100200), Yunnan Revitalization Talent Support Program “Young Talent” and “Innovation Team” (202405AS350019) Projects, the 14th Five-Year Plan of Xishuangbanna Tropical Botanical Garden, Chinese Academy of Sciences (XTBG-1450101) and the Key Programs of Yunnan Province, China (202103AC100003, 202101BC070003). We are grateful to Jie Cai, Li-Na Dong, Lian-Ming Gao, Hua-Jie He, Wei Jiang, Rong Li, Bin Liu, En-De Liu, Jie Liu, Min-Lu Liu, Lu Lu, Yang Luo, Hui Tang, Chun-Lei Xiang, Ji-Dong Ya, Qiu-Lin Yang, Xiu-Long Yang and Shu-Dong Zhang for their help in the field work and/or providing plant samples, to Jing Yang and Zhi-Rong Zhang for their help and suggestions in the lab work, and for the physical support from the Germplasm Bank of Wild Species, Kunming Institute of Botany, Chinese Academy of Sciences, and the Information Center, Xishuangbanna Tropical Botanical Garden, Chinese Academy of Sciences.

Conflict of interest

The authors declare no conflict of interest.

Data availability

The datasets presented in this study can be found in online repositories. The names of the repository/repositories and accession number(s) can be found in the article/Supplementary Material.

References

Aguirre-Santoro, J., Salinas, N.R. and Michelangeli, F.A., 2020. The influence of floral variation and geographic disjunction on the evolutionary dynamics of *Ronnbergia* and *Wittmackia* (Bromeliaceae: Bromelioideae). Bot. J. Linn. Soc. 192, 609–624.

Antonelli, A., Kissling, W.D., Flantua, S.G.A., Bermudez, M.A., Mulch, A., Muellner-Riehl, A.N., Kreft, H., Linder, H.P., Badgley, C., Fjeldsa, J., Fritz, S.A., Rahbek, C., Herman, F., Hooghiemstra, H. and Hoorn, C., 2018. Geological and climatic influences on mountain biodiversity. Nat. Geosci. 11, 718–725.

Armbruster, W.S., 2014. Floral specialization and angiosperm diversity: phenotypic divergence, fitness trade-offs and realized pollination accuracy. AoB PLANTS 6, plu003.

Armbruster, W.S. and Muchhala, N., 2009. Associations between floral specialization and species diversity: cause, effect, or correlation? Evol. Ecol. 23, 159–179.

Armbruster, W.S., Shi, X.-Q. and Huang, S.-Q., 2014. Do specialized flowers promote reproductive isolation? Realized pollination accuracy of three sympatric *Pedicularis* species. Ann. Bot. 113, 331–340.

Beaulieu, J.M., O’Meara, B.C. and Donoghue, M.J., 2013. Identifying hidden rate changes in the evolution of a binary morphological character: the evolution of plant habit in campanulid angiosperms. Syst. Biol. 62, 725–737.

Bivand, R.S. and Wong, D.W.S., 2018. Comparing implementations of global and local indicators of spatial association. Test 27, 716–748.

Boufford, D.E., 2014. Biodiversity hotspot: China's Hengduan Mountains. Arnoldia 72, 24–35.

Boyko, J.D. and Beaulieu, J.M., 2021. Generalized hidden Markov models for phylogenetic comparative datasets. Methods Ecol. Evol. 12, 468–478.

Cao, K., Wang, G., Leloup, P.H., Mahéo, G., Xu, Y., van der Beek, P.A., Replumaz, A. and Zhang, K., 2019. Oligocene-Early Miocene topographic relief generation of southeastern Tibet triggered by thrusting. Tectonics 38, 374–391.

Cao, K., Tian, Y., van der Beek, P., Wang, G., Shen, T., Reiners, P., Bernet, M. and Husson, L., 2022. Southwestward growth of plateau surfaces in eastern Tibet. Earth Sci. Rev. 232, 104160.

Capella-Gutierrez, S., Silla-Martinez, J.M. and Gabaldon, T., 2009. trimAl: a tool for automated alignment trimming in large-scale phylogenetic analyses. Bioinformatics 25, 1972–1973.

Chang, Y., Gelwick, K., Willett, S.D., Shen, X., Albouy, C., Luo, A., Wang, Z., Zimmermann, N.E. and Pellissier, L., 2023. Phytodiversity is associated with habitat heterogeneity from Eurasia to the Hengduan Mountains. New Phytol. 240, 1647–1658.

Chen, J.-T., Lidén, M., Huang, X.-H., Zhang, L., Zhang, X.-J., Kuang, T.-H., Landis, J.B., Wang, D., Deng, T. and Sun, H., 2023. An updated classification for the hyper-diverse genus *Corydalis* (Papaveraceae: Fumarioideae) based on phylogenomic and morphological evidence. J. Integr. Plant Biol. 65, 2138–2156.

Clark, M.K. and Royden, L.H., 2000. Topographic ooze: building the eastern margin of Tibet by lower crustal flow. Geology 28, 703–706.

Clark, M.K., Schoenbohm, L.M., Royden, L.H., Whipple, K.X., Burchfiel, B.C., Zhang, X., Tang, W., Wang, E. and Chen, L., 2004. Surface uplift, tectonics, and erosion of eastern Tibet from large-scale drainage patterns. Tectonics 23, TC1006.

Clark, M.K., House, M.A., Royden, L.H., Whipple, K.X., Burchfiel, B.C., Zhang, X. and Tang, W., 2005. Late Cenozoic uplift of southeastern Tibet. Geology 33, 525–528.

Darriba, D., Taboada, G.L., Doallo, R. and Posada, D., 2012. jModelTest 2: more models, new heuristics and parallel computing. Nat. Methods 9, 772.

De Kort, H., Panis, B., Helsen, K., Douzet, R., Janssens, S.B. and Honnay, O., 2020. Pre-adaptation to climate change through topography-driven phenotypic plasticity. J. Ecol. 108, 1465–1474.

Ding, L., Spicer, R.A., Yang, J., Xu, Q., Cai, F., Li, S., Lai, Q., Wang, H., Spicer, T.E.V., Yue, Y., Shukla, A., Srivastava, G., Khan, M.A., Bera, S. and Mehrotra, R., 2017. Quantifying the rise of the Himalaya orogen and implications for the South Asian monsoon. Geology 45, 215–218.

Ding, W.-N., Ree, R.H., Spicer, R.A. and Xing, Y.-W., 2020. Ancient orogenic and monsoon-driven assembly of the world's richest temperate alpine flora. Science 369, 578–581.

Drummond, C.S., Eastwood, R.J., Miotto, S.T.S. and Hughes, C.E., 2012. Multiple continental radiations and correlates of diversification in *Lupinus* (Leguminosae): testing for key innovation with incomplete taxon sampling. Syst. Biol. 61, 443–460.

Eaton, D.A.R., Fenster, C.B., Hereford, J., Huang, S.-Q. and Ree, R.H., 2012. Floral diversity and community structure in *Pedicularis* (Orobanchaceae). Ecology 93, S182–S194.

Farnsworth, A., Lunt, D.J., Robinson, S.A., Valdes, P.J., Roberts, W.H.G., Clift, P.D., Markwick, P., Su, T., Wrobel, N., Bragg, F., Kelland, S.-J. and Pancost, R.D., 2019. Past East Asian monsoon evolution controlled by paleogeography, not CO2. Science. Advances 5, eaax1697.

Fick, S.E. and Hijmans, R.J., 2017. WorldClim 2: new 1-km spatial resolution climate surfaces for global land areas. Int. J. Climatol. 37, 4302–4315.

FitzJohn, R.G., 2012. Diversitree: comparative phylogenetic analyses of diversification in R. Methods Ecol. Evol. 3, 1084–1092.

Garcia-Porta, J., Sol, D., Pennell, M., Sayol, F., Kaliontzopoulou, A. and Botero, C.A., 2022. Niche expansion and adaptive divergence in the global radiation of crows and ravens. Nat. Commun. 13, 2086.

Gébelin, A., Mulch, A., Teyssier, C., Jessup, M.J., Law, R.D. and Brunel, M., 2013. The Miocene elevation of Mount Everest. Geology 41, 799–802.

Givnish, T.J., 2015. Adaptive radiation versus 'radiation' and 'explosive diversification': why conceptual distinctions are fundamental to understanding evolution. New Phytol. 207, 297–303.

Givnish, T.J., Barfuss, M.H.J., Van Ee, B., Riina, R., Schulte, K., Horres, R., Gonsiska, P.A., Jabaily, R.S., Crayn, D.M., Smith, J.A.C., Winter, K., Brown, G.K., Evans, T.M., Holst, B.K., Luther, H., Till, W., Zizka, G., Berry, P.E. and Sytsma, K.J., 2014. Adaptive radiation, correlated and contingent evolution, and net species diversification in Bromeliaceae. Mol. Phylogenet. Evol. 71, 55–78.

Glor, R.E., 2010. Phylogenetic insights on adaptive radiation. Annu. Rev. Ecol. Evol. Syst. 41, 251–270.

Goloboff, P.A. and Morales, M.E., 2023. TNT version 1.6, with a graphical interface for MacOS and Linux, including new routines in parallel. Cladistics 39, 144–153.

Goloboff, P.A., Farris, J.S. and Nixon, K.C., 2008. TNT, a free program for phylogenetic analysis. Cladistics 24, 774–786.

Grant, V., 1994a. Mechanical and ethological isolation between *Pedicularis groenlandica* and *P. attollens* (Scrophulariaceae). Biol. Zent. Bl. 113, 43–51.

Grant, V., 1994b. Modes and origins of mechanical and ethological isolation in angiosperms. Proc. Natl. Acad. Sci. USA 91, 3–10.

Harder, L.D., 1990. Pollen removal by bumble bees and its implications for pollen dispersal. Ecology 71, 1110–1125.

He, K. and Jiang, X., 2014. Sky islands of southwest China. I: an overview of phylogeographic patterns. Chin. Sci. Bull. 59, 585–597.

Ho, S.Y.W., 2020. The molecular clock and evolutionary rates across the tree of life. In: Ho, S.Y.W. (Ed.), The Molecular Evolutionary Clock: Theory and Practice. Springer International Publishing, Cham, pp. 3–23.

Ho, S.Y.W., Lanfear, R., Bromham, L., Phillips, M.J., Soubrier, J., Rodrigo, A.G. and Cooper, A., 2011. Time-dependent rates of molecular evolution. Mol. Ecol. 20, 3087–3101.

Höhna, S., Landis, M.J., Heath, T.A., Boussau, B., Lartillot, N., Moore, B.R., Huelsenbeck, J.P. and Ronquist, F., 2016. RevBayes: Bayesian Phylogenetic Inference using graphical models and an interactive model-specification language. Syst. Biol. 65, 726–736.

Hoorn, C., Mosbrugger, V., Mulch, A. and Antonelli, A., 2013. Biodiversity from mountain building. Nat. Geosci. 6, 154.

Huang, S.-Q. and Shi, X.-Q., 2013. Floral isolation in *Pedicularis*: how do congeners with shared pollinators minimize reproductive interference? New Phytol. 199, 858–865.

Jiang, N., Dong, L.-N., Yang, J.-B., Tan, Y.-H., Wang, H., Randle, C.P., Li, D.-Z. and Yu, W.-B., 2022. Herbarium phylogenomics: resolving the generic status of the enigmatic *Pseudobartsia* (Orobanchaceae). J. Syst. Evol. 60, 1218–1228.

Jin, J.-J., Yu, W.-B., Yang, J.-B., Song, Y., dePamphilis, C.W., Yi, T.-S. and Li, D.-Z., 2020. GetOrganelle: a fast and versatile toolkit for accurate de novo assembly of organelle genomes. Genome Biol. 21, 241.

John, F. and Sanford, W., 2019. An R Companion to Applied Regression. Sage, Thousand Oaks CA.

Katoh, K., Rozewicki, J. and Yamada, K.D., 2019. MAFFT online service: multiple sequence alignment, interactive sequence choice and visualization. Brief. Bioinform. 20, 1160–1166.

Kearse, M., Moir, R., Wilson, A., Stones-Havas, S., Cheung, M., Sturrock, S., Buxton, S., Cooper, A., Markowitz, S., Duran, C., Thierer, T., Ashton, B., Meintjes, P. and Drummond, A., 2012. Geneious Basic: an integrated and extendable desktop software platform for the organization and analysis of sequence data. Bioinformatics 28, 1647–1649.

Lagomarsino, L.P., Condamine, F.L., Antonelli, A., Mulch, A. and Davis, C.C., 2016. The abiotic and biotic drivers of rapid diversification in Andean bellflowers (Campanulaceae). New Phytol. 210, 1430–1442.

Lee, J.-Y., Wang, B., Seo, K.-H., Ha, K.-J., Kitoh, A. and Liu, J., 2015. Effects of mountain uplift on global monsoon precipitation. Asia-Pac. J. Atmos. Sci. 51, 275–290.

Li, H.-L., 1948. A revision of the genus *Pedicularis* in China. part I. Proc. Acad. Natl. Sci. Phila. 100, 205–378.

Li, H.-L., 1949. A revision of the genus *Pedicularis* in China. part II. Proc. Acad. Natl. Sci. Phila. 101, 1–378.

Li, Y., Zhai, S.-N., Qiu, Y.-X., Guo, Y.-P., Ge, X.-J. and Comes, H.P., 2011. Glacial survival east and west of the 'Mekong–Salween Divide' in the Himalaya–Hengduan Mountains region as revealed by AFLPs and cpDNA sequence variation in *Sinopodophyllum hexandrum* (Berberidaceae). Mol. Phylogenet. Evol. 59, 412–424.

Li, A.-R., Smith, F.A., Smith, S.E. and Guan, K.-Y., 2012. Two sympatric root hemiparasitic *Pedicularis* species differ in host dependency and selectivity under phosphorus limitation. Funct. Plant Biol. 39, 784–794.

Li, M., Zhang, X.Z., Niu, B., He, Y.T., Wang, X.T. and Wu, J.S., 2020. Changes in plant species richness distribution in Tibetan alpine grasslands under different precipitation scenarios. Glob. Ecol. Conserv. 21, e00848.

Li, Q., Sun, H., Boufford, D.E., Bartholomew, B., Fritsch, P.W., Chen, J., Deng, T. and Ree, R.H., 2021a. Grade of Membership models reveal geographical and environmental correlates of floristic structure in a temperate biodiversity hotspot. New Phytol. 232, 1424–1435.

Li, X., Yang, J.-B., Wang, H., Song, Y., Corlett, R.T., Yao, X., Li, D.-Z. and Yu, W.-B., 2021b. Plastid NDH pseudogenization and gene loss in a recently derived lineage from the largest hemiparasitic plant genus *Pedicularis* (Orobanchaceae). Plant Cell Physiol. 62, 971–984.

Liu, M.-L., Yu, W.-B., Kuss, P., Li, D.-Z. and Wang, H., 2015. Floral nectary morphology and evolution in *Pedicularis* (Orobanchaceae). Bot. J. Linn. Soc. 178, 592–607.

Liu, Y.-N., Li, Y., Yang, F.-S. and Wang, X.-Q., 2016. Floral nectary, nectar production dynamics, and floral reproductive isolation among closely related species of *Pedicularis*. J. Integr. Plant Biol. 58, 178–187.

Liu, Y., Ye, J.-F., Hu, H.-H., Peng, D.-X., Zhao, L.-N., Lu, L.-M., Zaman, W. and Chen, Z.-D., 2021. Influence of elevation on bioregionalisation: a case study of the Sino-Himalayan flora. J. Biogeogr. 48, 2578–2587.

Liu, J., Milne, R.I., Zhu, G.-F., Spicer, R.A., Wambulwa, M.C., Wu, Z.-Y., Boufford, D.E., Luo, Y.-H., Provan, J., Yi, T.-S., Cai, J., Wang, H., Gao, L.-M. and Li, D.-Z., 2022a. Name and scale matter: clarifying the geography of Tibetan Plateau and adjacent mountain regions. Glob. Planet. Chang. 215, 103893.

Liu, R., Wang, H., Yang, J.-B., Corlett, R.T., Randle, C.P., Li, D.-Z. and Yu, W.-B., 2022b. Cryptic species diversification of the *Pedicularis siphonantha* Complex (Orobanchaceae) in the mountains of Southwest China since the Pliocene. Front. Plant Sci. 13, 811206.

Liu-Zeng, J., Tapponnier, P., Gaudemer, Y. and Ding, L., 2008. Quantifying landscape differences across the Tibetan plateau: implications for topographic relief evolution. J. Geophys. Res. Earth 113, F04018.

Louca, S., Henao-Diaz, L.F. and Pennell, M., 2022. The scaling of diversification rates with age is likely explained by sampling bias. Evolution 76, 1625–1637.

Luo, D., Xu, B., Li, Z.M. and Sun, H., 2017. The 'Ward Line-Mekong-Salween Divide' is an important floristic boundary between the eastern Himalaya and Hengduan Mountains: evidence from the phylogeographical structure of subnival herbs *Marmoritis complanatum* (Lamiaceae). Bot. J. Linn. Soc. 185, 482–496.

Macior, L., 1982. Plant community and pollinator dynamics in the evolution of pollination mechanisms in *Pedicularis* (Scrophulariaceae). In: Armstrong, J.A., Powell, J. and Richards, A.J. (Eds.), Pollination and evolution. Royal Botanic Gardens, Sydney, NSW, pp. 29–45.

Macior, L.W. and Ya, T., 1997. A preliminary study of the pollination ecology of *Pedicularis* in the Chinese Himalaya. Plant Species Biol. 12, 1–7.

McNeal, J.R., Bennett, J.R., Wolfe, A.D. and Mathews, S., 2013. Phylogeny and origins of holoparasitism in Orobanchaceae. Am. J. Bot. 100, 971–983.

Mo, Z.-Q., Fu, C.-N., Zhu, M.-S., Milne, R.I., Yang, J.-B., Cai, J., Qin, H.-T., Zheng, W., Hollingsworth, P.M., Li, D.-Z. and Gao, L.-M., 2022. Resolution, conflict and rate shifts: insights from a densely sampled plastome phylogeny for *Rhododendron* (Ericaceae). Ann. Bot. 130, 687–701.

Moen, D. and Morlon, H., 2014. Why does diversification slow down? Trends Ecol. Evol. 29, 190–197.

Morlon, H., Lewitus, E., Condamine, F.L., Manceau, M., Clavel, J. and Drury, J., 2016. RPANDA: an R package for macroevolutionary analyses on phylogenetic trees. Methods Ecol. Evol. 7, 589–597.

Mu, Q.Y., Yu, C.C., Wang, Y., Han, T.S., Wang, H., Ding, W.N., Zhang, Q.Y., Low, S.L., Zheng, Q.J., Peng, C.A., Hu, Z.Y. and Xing, Y.W., 2022. Comparative phylogeography of *Acanthocalyx* (Caprifoliaceae) reveals distinct genetic structures in the Himalaya-Hengduan Mountains. Alp. Bot. 132, 153–168.

Mulch, A., 2016. Stable isotope paleoaltimetry and the evolution of landscapes and life. Earth Planet. Sci. Lett. 433, 180–191.

Nie, J., Ruetenik, G., Gallagher, K., Hoke, G., Garzione, C.N., Wang, W., Stockli, D., Hu, X., Wang, Z., Wang, Y., Stevens, T., Danišík, M. and Liu, S., 2018. Rapid incision of the Mekong River in the middle Miocene linked to monsoonal precipitation. Nat. Geosci. 11, 944–948.

Pahlich, E. and Gerlitz, C., 1980. A rapid DNA isolation procedure for small quantities of fresh leaf tissue. Phytochemistry 19, 11–13.

Paradis, E., Claude, J. and Strimmer, K., 2004. APE: analyses of phylogenetics and evolution in R language. Bioinformatics 20, 289–290.

Pennell, M.W., Eastman, J.M., Slater, G.J., Brown, J.W., Uyeda, J.C., FitzJohn, R.G., Alfaro, M.E. and Harmon, L.J., 2014. geiger v2.0: an expanded suite of methods for fitting macroevolutionary models to phylogenetic trees. Bioinformatics 30, 2216–2218.

Pepin, N.C., Arnone, E., Gobiet, A., Haslinger, K., Kotlarski, S., Notarnicola, C., Palazzi, E., Seibert, P., Serafin, S., Schöner, W., Terzago, S., Thornton, J.M., Vuille, M. and Adler, C., 2022. Climate changes and their elevational patterns in the mountains of the world. Rev. Geophys. 60, e2020RG000730.

Perrigo, A., Hoorn, C. and Antonelli, A., 2020. Why mountains matter for biodiversity. J. Biogeogr. 47, 315–325.

Pigot, A.L., Phillimore, A.B., Owens, I.P.F. and Orme, C.D.L., 2010. The shape and temporal dynamics of phylogenetic trees arising from geographic speciation. Syst. Biol. 59, 660–673.

Plummer, M., Best, N., Cowles, K. and Vines, K., 2006. CODA: convergence diagnosis and output analysis for MCMC. R News 6, 7–11.

Qu, X.-J., Moore, M.J., Li, D.-Z. and Yi, T.-S., 2019. PGA: a software package for rapid, accurate, and flexible batch annotation of plastomes. Plant Methods 15, 50.

Rabosky, D.L., 2014. Automatic detection of key Innovations, rate shifts, and diversity-dependence on phylogenetic trees. PLoS One 9, e89543.

Rabosky, D.L. and Lovette, I.J., 2008. Density-dependent diversification in North American wood warblers. Proc. R. Soc. B Biol. Sci. 275, 2363–2371.

Rabosky, D.L., Grundler, M., Anderson, C., Title, P., Shi, J.J., Brown, J.W., Huang, H. and Larson, J.G., 2014. BAMMtools: an R package for the analysis of evolutionary dynamics on phylogenetic trees. Methods Ecol. Evol. 5, 701–707.

Rahbek, C., Borregaard, M.K., Antonelli, A., Colwell, R.K., Holt, B.G., Nogues-Bravo, D., Rasmussen, C.M.Ø., Richardson, K., Rosing, M.T., Whittaker, R.J. and Fjeldså, J., 2019a. Building mountain biodiversity: geological and evolutionary processes. Science 365, 1114–1119.

Rahbek, C., Borregaard, M.K., Colwell, R.K., Dalsgaard, B., Holt, B.G., Morueta-Holme, N., Nogues-Bravo, D., Whittaker, R.J. and Fjeldsa, J., 2019b. Humboldt's enigma: what causes global patterns of mountain biodiversity? Science 365, 1108–1113.

Rambaut, A., Drummond, A.J., Xie, D., Baele, G. and Suchard, M.A., 2018. Posterior summarization in Bayesian phylogenetics using Tracer 1.7. Syst. Biol. 67, 901–904.

Rana, H.K., Rana, S.K., Luo, D. and Sun, H., 2023. Existence of biogeographic barriers for the long-term Neogene-Quaternary divergence and differentiation of *Koenigia forrestii* in the Himalaya-Hengduan Mountains. Bot. J. Linn. Soc. 201, 230–253.

Ree, R.H., 2005. Phylogeny and the evolution of floral diversity in *Pedicularis* (Orobanchaceae). Int. J. Plant Sci. 166, 595–613.

Ree, R.H. and Sanmartín, I., 2018. Conceptual and statistical problems with the DEC+J model of founder-event speciation and its comparison with DEC via model selection. J. Biogeogr. 45, 741–749.

Ree, R.H. and Smith, S.A., 2008. Maximum likelihood inference of geographic range evolution by dispersal, local extinction, and cladogenesis. Syst. Biol. 57, 4–14.

Ren, Y.-Q., Guan, K.-Y., Li, A.-R., Hu, X.-J. and Zhang, L., 2010. Host dependence and preference of the root hemiparasite, *Pedicularis cephalantha* Franch. (Orobanchaceae). Folia Geobot. 45, 443–455.

Revell, L.J., 2012. phytools: an R package for phylogenetic comparative biology (and other things). Methods Ecol. Evol. 3, 217–223.

Revell, L.J., 2013. Two new graphical methods for mapping trait evolution on phylogenies. Methods Ecol. Evol. 4, 754–759.

Revell, L.J., 2024. phytools 2.0: an updated R ecosystem for phylogenetic comparative methods (and other things). PeerJ 12, e16505.

Ricklefs, R.E., 2010. Evolutionary diversification, coevolution between populations and their antagonists, and the filling of niche space. Proc. Natl. Acad. Sci. USA 107, 1265–1272.

Robart, B.W., 2005. Morphological diversification and taxonomy among the varieties of *Pedicularis bracteosa* Benth. (Orobanchaceae). Syst. Bot. 30, 644–656.

Ronquist, F., Teslenko, M., van der Mark, P., Ayres, D.L., Darling, A., Höhna, S., Larget, B., Liu, L., Suchard, M.A. and Huelsenbeck, J.P., 2012. MrBayes 3.2: efficient Bayesian Phylogenetic Inference and model choice across a large model space. Syst. Biol. 61, 539–542.

Skipwith, P.L., Bauer, A.M., Jackman, T.R. and Sadlier, R.A., 2016. Old but not ancient: coalescent species tree of New Caledonian geckos reveals recent post-inundation diversification. J. Biogeogr. 43, 1266–1276.

Spicer, R.A., Farnsworth, A. and Su, T., 2020. Cenozoic topography, monsoons and biodiversity conservation within the Tibetan Region: an evolving story. Plant Divers. 42, 229–254.

Spicer, R.A., Su, T., Valdes, P.J., Farnsworth, A., Wu, F.-X., Shi, G., Spicer, T.E.V. and Zhou, Z., 2021. Why 'the uplift of the Tibetan Plateau' is a myth. Natl. Sci. Rev. 8, nwaa091.

Stamatakis, A., 2014. RAxML version 8: a tool for phylogenetic analysis and post-analysis of large phylogenies. Bioinformatics 30, 1312–1313.

Su, T., Spicer, R.A., Li, S.-H., Xu, H., Huang, J., Sherlock, S., Huang, Y.-J., Li, S.-F., Wang, L., Jia, L.-B., Deng, W.-Y.-D., Liu, J., Deng, C.-L., Zhang, S.-T., Valdes, P.J. and Zhou, Z.-K., 2019. Uplift, climate and biotic changes at the Eocene–Oligocene transition in south-eastern Tibet. Natl. Sci. Rev. 6, 495–504.

Suchard, M.A., Lemey, P., Baele, G., Ayres, D.L., Drummond, A.J. and Rambaut, A., 2018. Bayesian phylogenetic and phylodynamic data integration using BEAST 1.10. Virus. Evolution 4, vey016.

Tkach, N., Ree, R.H., Kuss, P., Roeser, M. and Hoffmann, M.H., 2014. High mountain origin, phylogenetics, evolution, and niche conservatism of Arctic lineages in the hemiparasitic genus *Pedicularis* (Orobanchaceae). Mol. Phylogenet. Evol. 76, 75–92.

Tong, Z.-Y., Wang, X.-P., Wu, L.-Y. and Huang, S.-Q., 2019. Nectar supplementation changes pollinator behaviour and pollination mode in *Pedicularis dichotoma*: implications for evolutionary transitions. Ann. Bot. 123, 373–380.

Toussaint, E.F.A., Hendrich, L., Shaverdo, H. and Balke, M., 2015. Mosaic patterns of diversification dynamics following the colonization of Melanesian islands. Sci. Rep. 5, 16016.

TrÉNel, P., Hansen, M.M., Normand, S. and Borchsenius, F., 2008. Landscape genetics, historical isolation and cross-Andean gene flow in the wax palm, *Ceroxylon echinulatum* (Arecaceae). Mol. Ecol. 17, 3528–3540.

Tribble, C.M., Freyman, W.A., Landis, M.J., Lim, J.Y., Barido-Sottani, J., Kopperud, B.T., Höhna, S. and May, M.R., 2022. RevGadgets: an R package for visualizing Bayesian phylogenetic analyses from RevBayes. Methods Ecol. Evol. 13, 314–323.

Tsoong, P.-C., 1955. A new system for the genus *Pedicularis*. Zhi Wu Fen Lei Xue Bao 4, 71–147.

Tsoong, P.-C., 1956. A new system for the genus *Pedicularis*. Zhi Wu Fen Lei Xue Bao 5, 239–278.

Vieu, J.C., Hughes, C.E., Kissling, J. and Grant, J.R., 2022. Evolutionary diversification in the hyper-diverse montane forests of the tropical Andes: radiation of *Macrocarpaea* (Gentianaceae) and the possible role of range expansion. Bot. J. Linn. Soc. 199, 53–75.

Wang, H. and Li, D., 1998. A preliminary study of pollination biology of *Pedicularis* (Scrophulariaceae) in northwest Yunnan, China. Acta Bot. Sin. 40, 204–210.

Wang, H. and Li, D., 2005. Pollination biology of four *Pedicularis* species (Scrophulariaceae) in northwestern Yunnan, China. Ann. Mo. Bot. Gard. 92, 127–138.

Wellborn, G.A. and Langerhans, R.B., 2015. Ecological opportunity and the adaptive diversification of lineages. Ecol. Evol. 5, 176–195.

Wick, R.R., Schultz, M.B., Zobel, J. and Holt, K.E., 2015. Bandage: interactive visualization of de novo genome assemblies. Bioinformatics 31, 3350–3352.

Wu, C., 1988. Hengduan Mountains flora and her significance. J. Jap. Bot. (Journal of Japanese Botany) 63, 297–311.

Wu, Z., Zhou, Z., Sun, H., Li, D. and Peng, H., 2010. Floristics of Seed Plants from China. Science Press, Beijing.

Xia, X.-M., Yang, M.-Q., Li, C.-L., Huang, S.-X., Jin, W.-T., Shen, T.-T., Wang, F., Li, X.-H., Yoichi, W., Zhang, L.-H., Zheng, Y.-R. and Wang, X.-Q., 2022. Spatiotemporal evolution of the global species diversity of *Rhododendron*. Mol. Biol. Evol. 39, msab314.

Xing, Y. and Ree, R.H., 2017. Uplift-driven diversification in the Hengduan Mountains, a temperate biodiversity hotspot. Proc. Natl. Acad. Sci. USA 114, E3444–E3451.

Yang, F.S., Wang, X.Q. and Hong, D.Y., 2003. Unexpected high divergence in nrDNA ITS and extensive parallelism in floral morphology of *Pedicularis* (Orobanchaceae). Plant Syst. Evol. 240, 91–105.

Yang, C.-F., Gituru, R.W. and Guo, Y.-H., 2007. Reproductive isolation of two sympatric louseworts, *Pedicularis rhinanthoides* and *Pedicularis longiflora* (Orobanchaceae): how does the same pollinator type avoid interspecific pollen transfer? Biol. J. Linn. Soc. 90, 37–48.

Yang, F.S., Qin, A.L., Li, Y.F. and Wang, X.Q., 2012. Great genetic differentiation among populations of *Meconopsis integrifolia* and its implication for plant speciation in the Qinghai-Tibetan Plateau. PLoS One 7, e37196.

Ye, X.-Y., Ma, P.-F., Yang, G.-Q., Guo, C., Zhang, Y.-X., Chen, Y.-M., Guo, Z.-H. and Li, D.-Z., 2019. Rapid diversification of alpine bamboos associated with the uplift of the Hengduan Mountains. J. Biogeogr. 46, 2678–2689.

Yu, W.-B., Huang, P.-H., Li, D.-Z. and Wang, H., 2013. Incongruence between nuclear and chloroplast DNA phylogenies in *Pedicularis* section *Cyathophora* (Orobanchaceae). PLoS One 8, e74828.

Yu, W.B., Liu, M.L., Wang, H., Mill, R.R., Ree, R.H., Yang, J.B. and Li, D.Z., 2015. Towards a comprehensive phylogeny of the large temperate genus *Pedicularis* (Orobanchaceae), with an emphasis on species from the Himalaya-Hengduan Mountains. BMC Plant Biol. 15, 176.

Yu, W.-B., Randle, C.P., Lu, L., Wang, H., Yang, J.-B., Depamphilis, C.W., Corlett, R.T. and Li, D.-Z., 2018a. The hemiparasitic plant *Phtheirospermum* (Orobanchaceae) is polyphyletic and contains cryptic species in the Hengduan Mountains of southwest China. Front. Plant Sci. 9, 142.

Yu, W.-B., Wang, H., Liu, M.-L., Grabovskaya-Borodina, A.E. and Li, D.-Z., 2018b. Phylogenetic approaches resolve taxonomical confusion in *Pedicularis* (Orobanchaceae): reinstatement of *Pedicularis delavayi* and discovering a new species *Pedicularis milliana*. PLoS One 13, e0200372.

Yu, H., Miao, S., Xie, G., Guo, X., Chen, Z. and Favre, A., 2020. Contrasting floristic diversity of the Hengduan Mountains, the Himalayas and the Qinghai-Tibet Plateau sensu stricto in China. Front. Ecol. Evol. 8, 136.

Zachos, J.C., Dickens, G.R. and Zeebe, R.E., 2008. An early Cenozoic perspective on greenhouse warming and carbon-cycle dynamics. Nature 451, 279–283.

Zhang, D.-C., Ye, J.-X. and Sun, H., 2016. Quantitative approaches to identify floristic units and centres of species endemism in the Qinghai-Tibetan Plateau, south-western China. J. Biogeogr. 43, 2465–2476.

Zhang, D., Hao, G.-Q., Guo, X.-Y., Hu, Q.-J. and Liu, J.-Q., 2019. Genomic insight into “sky Island” species diversification in a mountainous biodiversity hotspot. J. Syst. Evol. 57, 633–645.

Zhang, X., Landis, J.B., Sun, Y., Zhang, H., Lin, N., Kuang, T., Huang, X., Deng, T., Wang, H. and Sun, H., 2021. Macroevolutionary pattern of *Saussurea* (Asteraceae) provides insights into the drivers of radiating diversification. Proc. R. Soc. B Biol. Sci. 288, 20211575.

Supporting Information

Additional supporting information may be found online in the Supporting Information section at the end of the article.

Fig. S1. RAxML-derived maximum likelihood (ML) tree for *Pedicularis* Clade 3 based on whole plastome sequences.

Fig. S2. RAxML-derived maximum likelihood (ML) tree for *Pedicularis* Clade 3 based on plastid coding region.

Fig. S3. TNT-derived strict consensus maximum parsimony (MP) tree with bootstrap sampling for *Pedicularis* Clade 3 based on plastid coding region.

Fig. S4. MrBayes-derived Bayesian inference (BI) for *Pedicularis* Clade 3 based on plastid coding region.

Fig. S5. BEAST-derived chronogram for *Pedicularis* Clade 3 based on plastid coding region.

Fig. S6. Evolutionary traitgram of elevation for *Pedicularis* Clade 3.

Fig. S7. Plots showing the estimated net diversification rates through time (a) and Asian monsoon change (b) estimated by RPANDA.

Fig. S8. Transition rate of different corolla type and rate class of corolla reconstruction.

Table S1. Species list in *Pedicularis* Clade 3.

Table S2. Plastid information of *Pedicularis* Clade 3.

Table S3. Species record of *Pedicularis* Clade 3.

Table S4. Morphological and ecological characters of *Pedicularis* Clade 3.

Table S5. Prior constraint of different corolla type in MuSSE model.

Table S6. Distribution overlap index and comparison of elevation and corolla traits of sister pair.

Table S7. Time-dependent and palaeoenvironment-dependent diversification models of RPANDA.